Precision photometry redward of K-band with a 'wall-eyed' pointing mode

Eckhart Spalding
LBTO 2017 User's Meeting
Florence, June 23

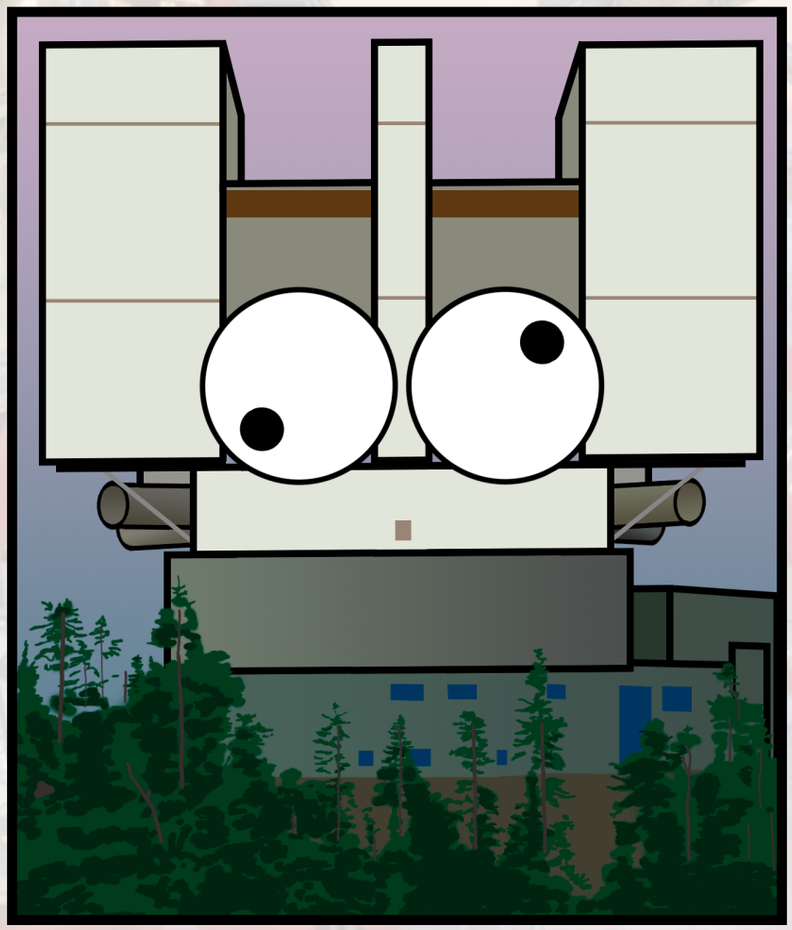

Chamber Image: Marc-André Besel & Wiphu Rujopakarn

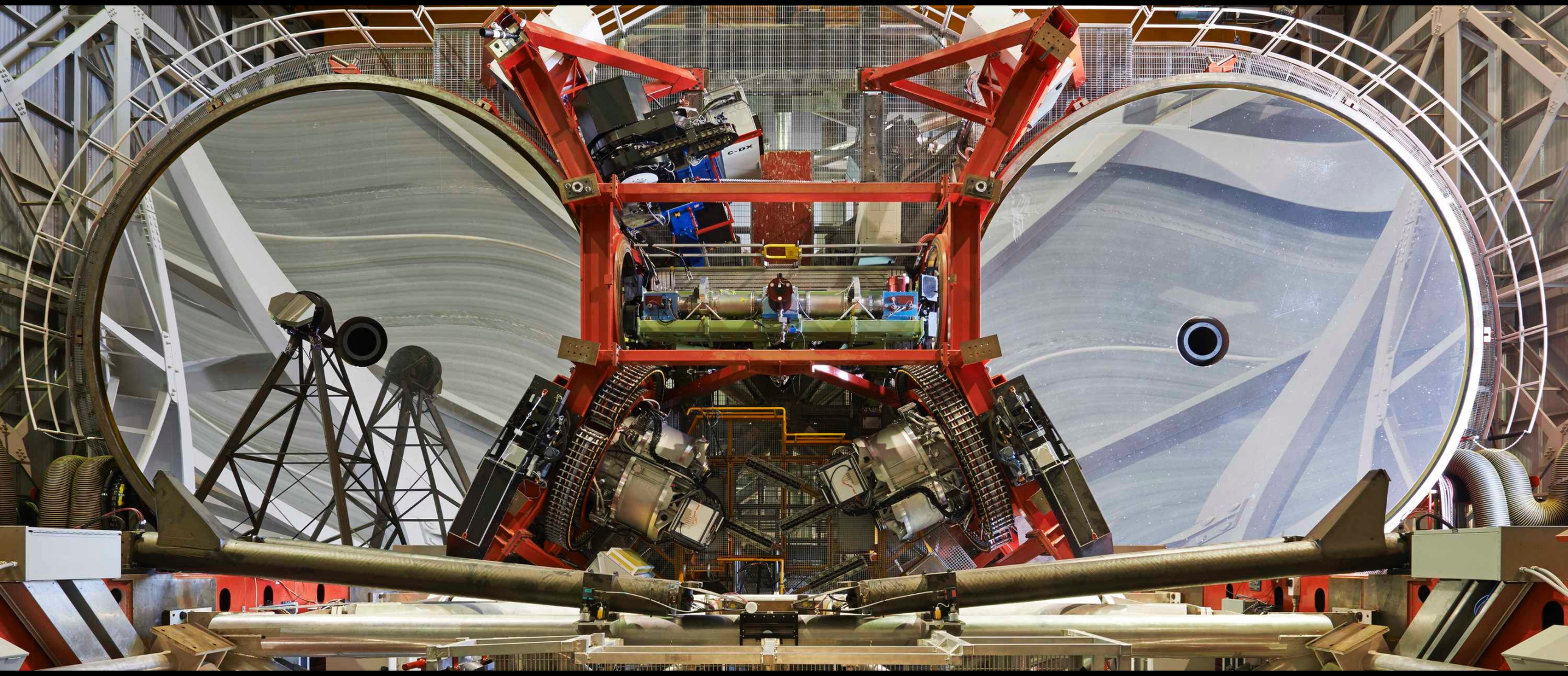

LBTO, Enrico Sacchetti

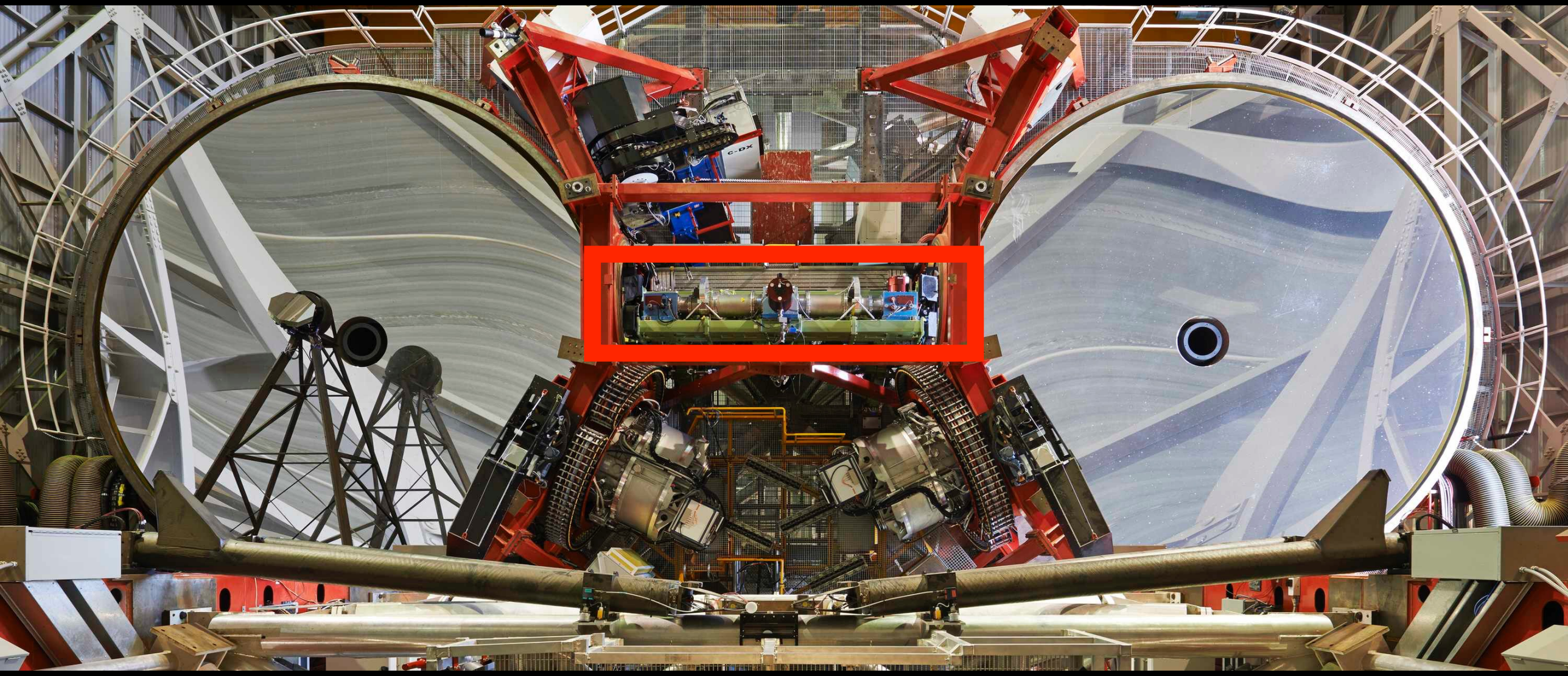

LBTO, Enrico Sacchetti

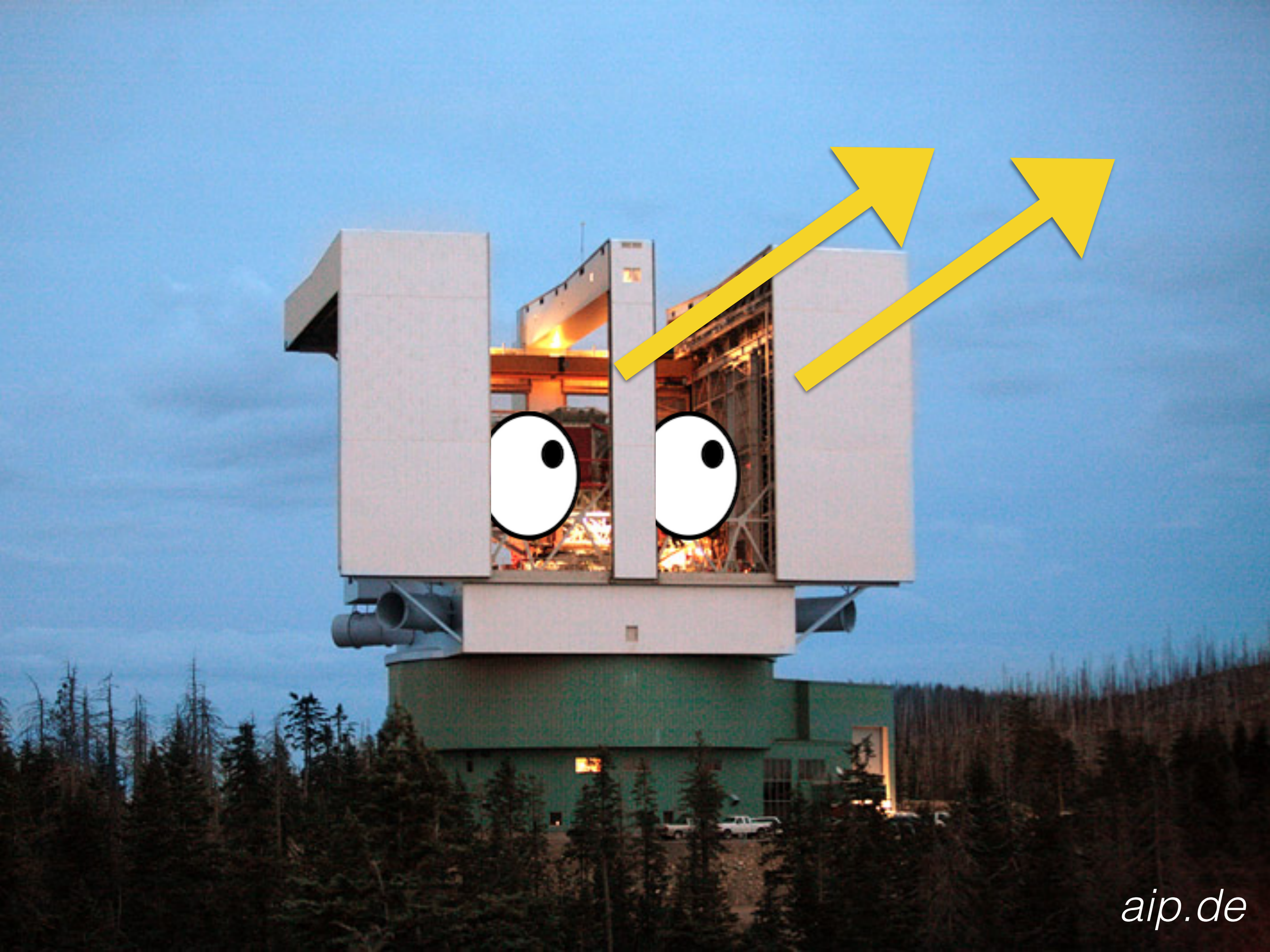

aip.de

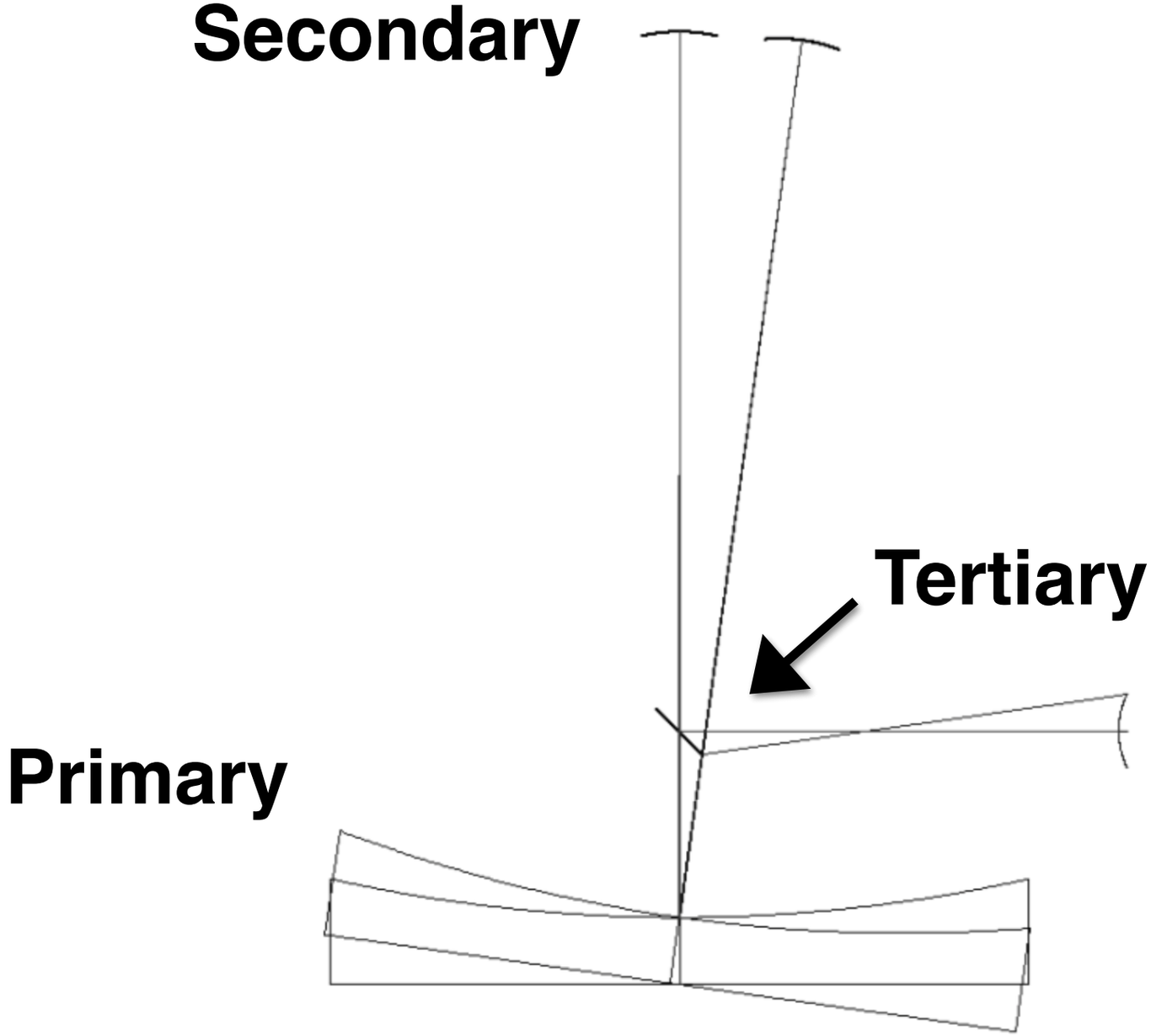

Fig. 3 in Rakich+ 2011

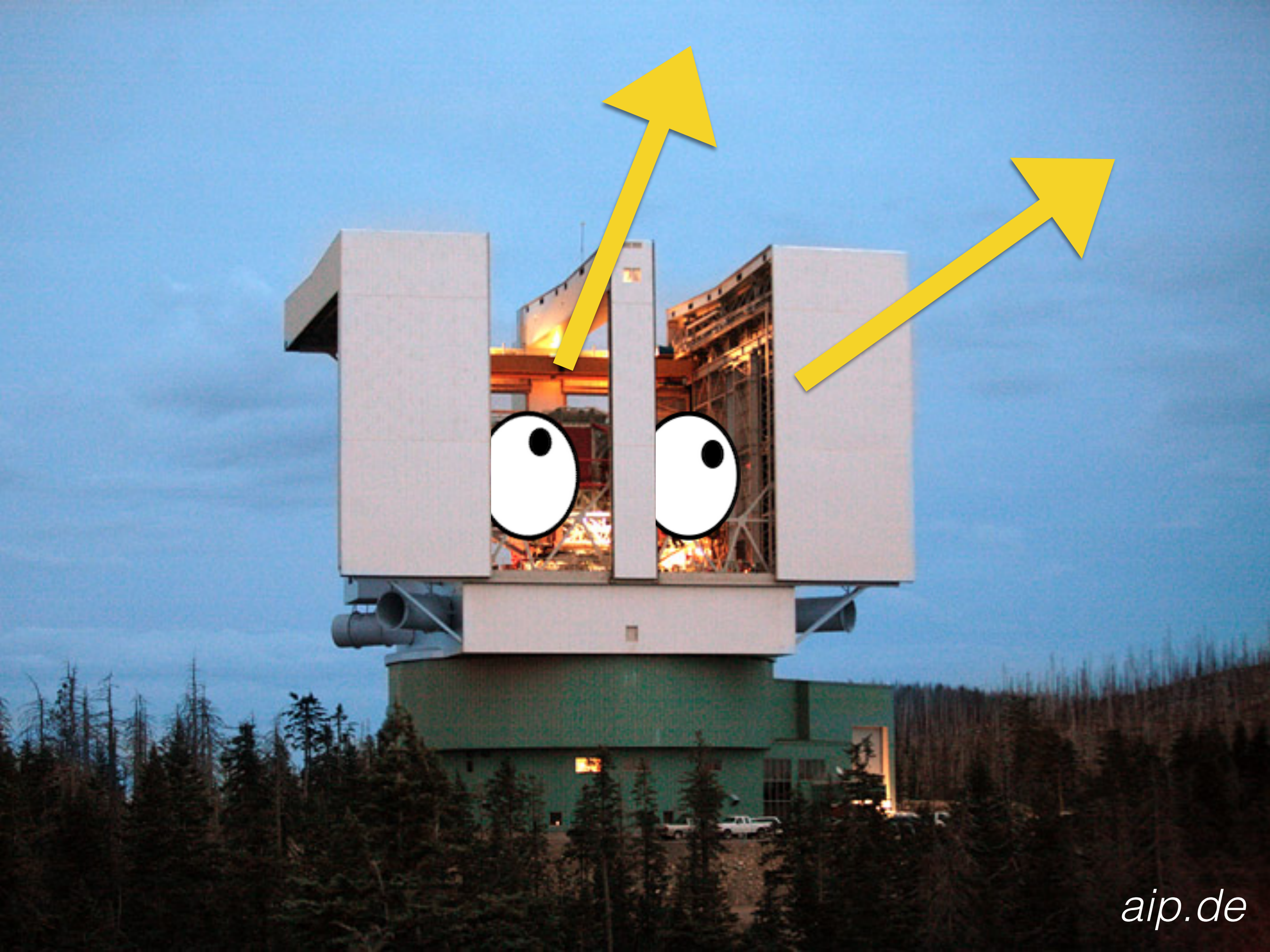

aip.de

1. The sky introduces a lot of noise

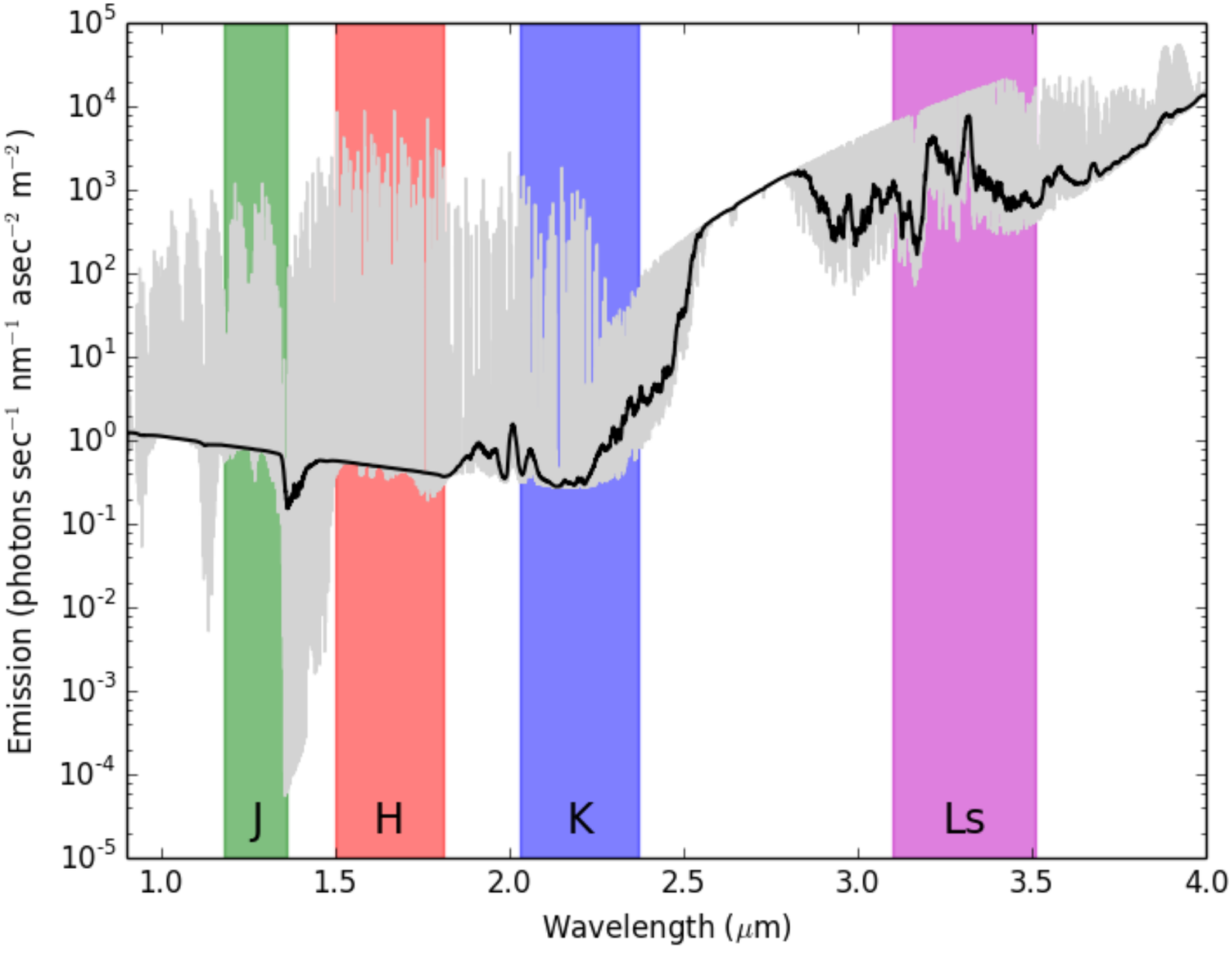

Emission data from Gemini Observatory

2. Fields-of-view are too small

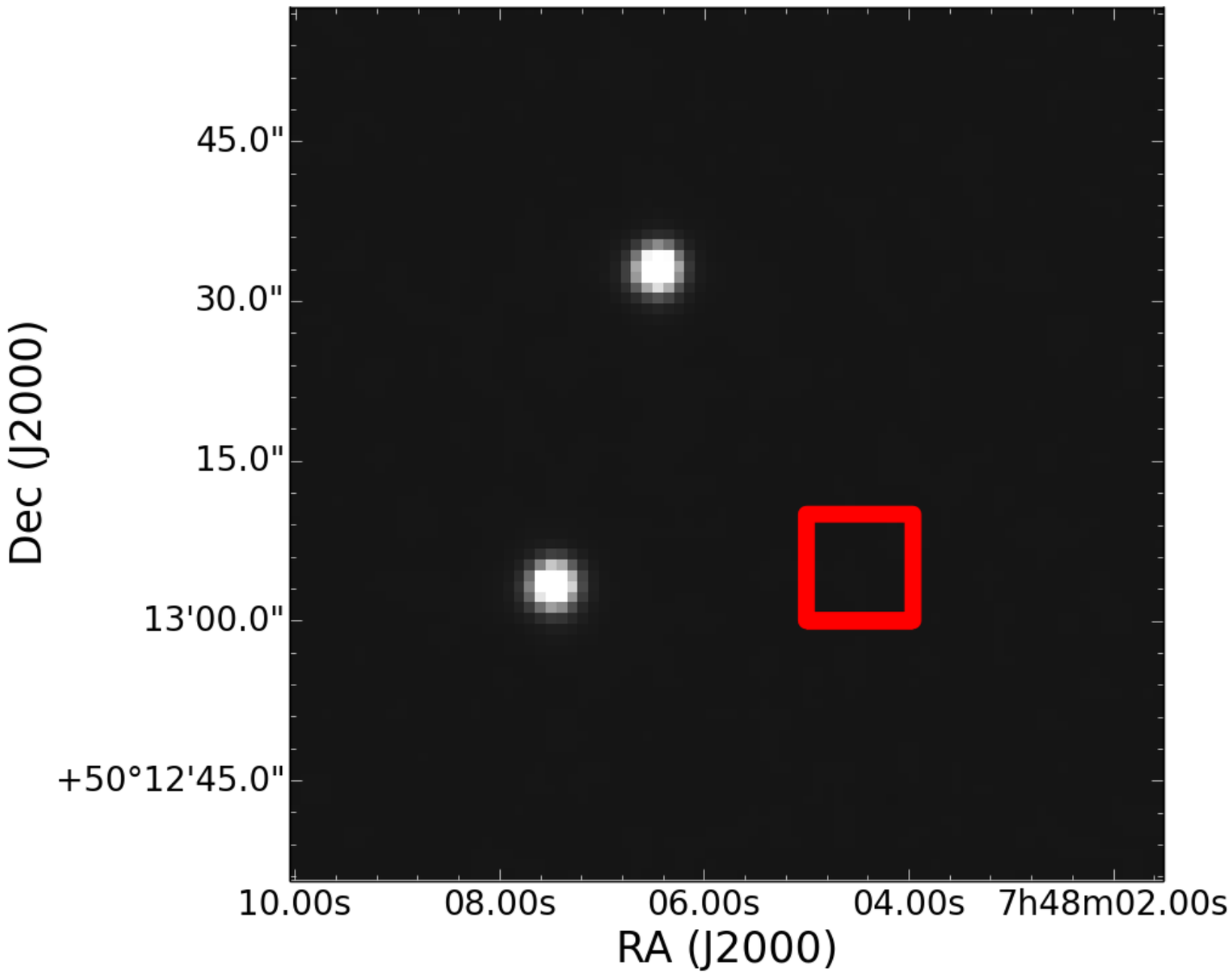

2MASS + NASA

2. Fields-of-view are too small

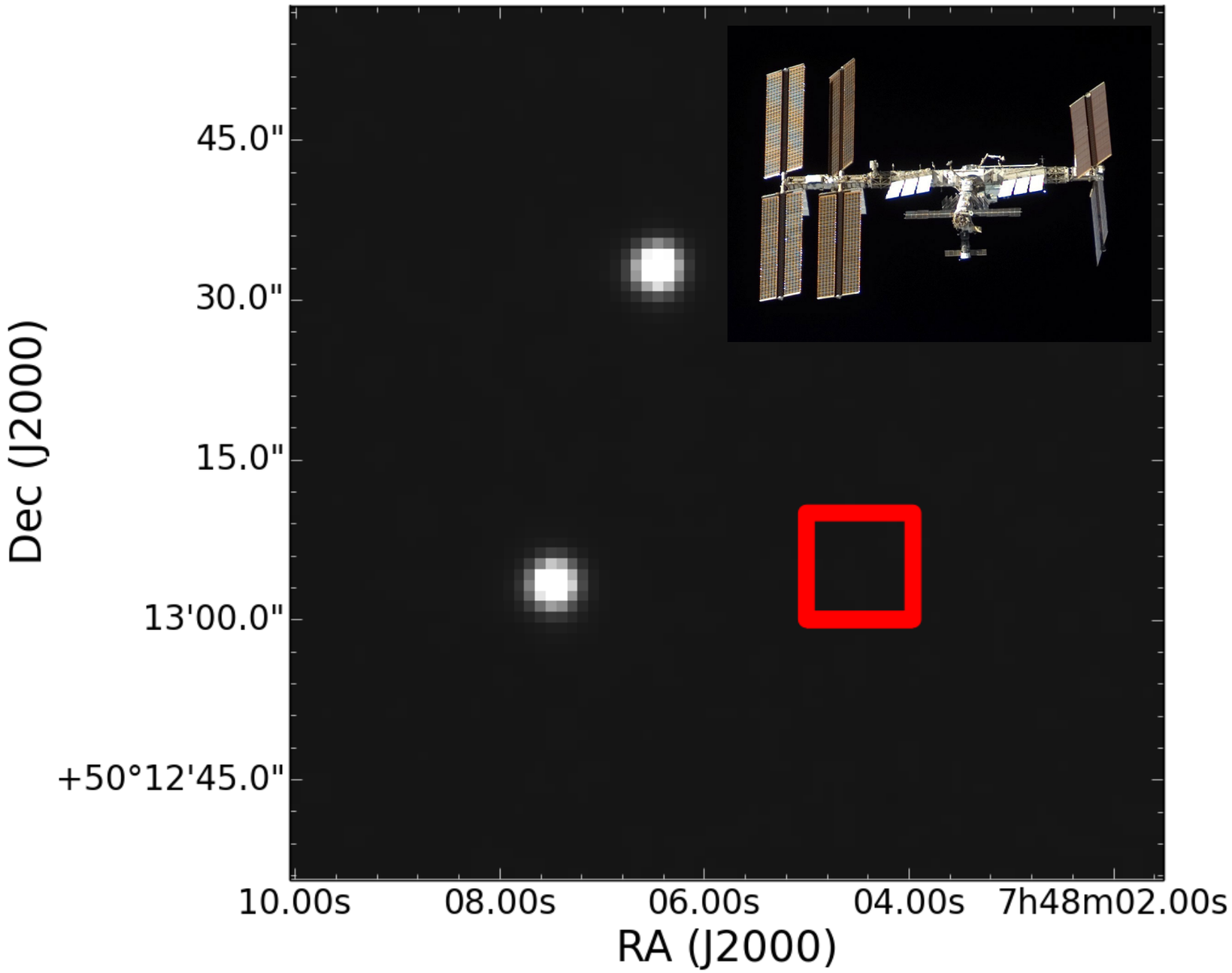

2MASS + NASA

Constant Targets	Primary Transit	Secondary Eclipse
HR 567+	XO-2	HD 189733+

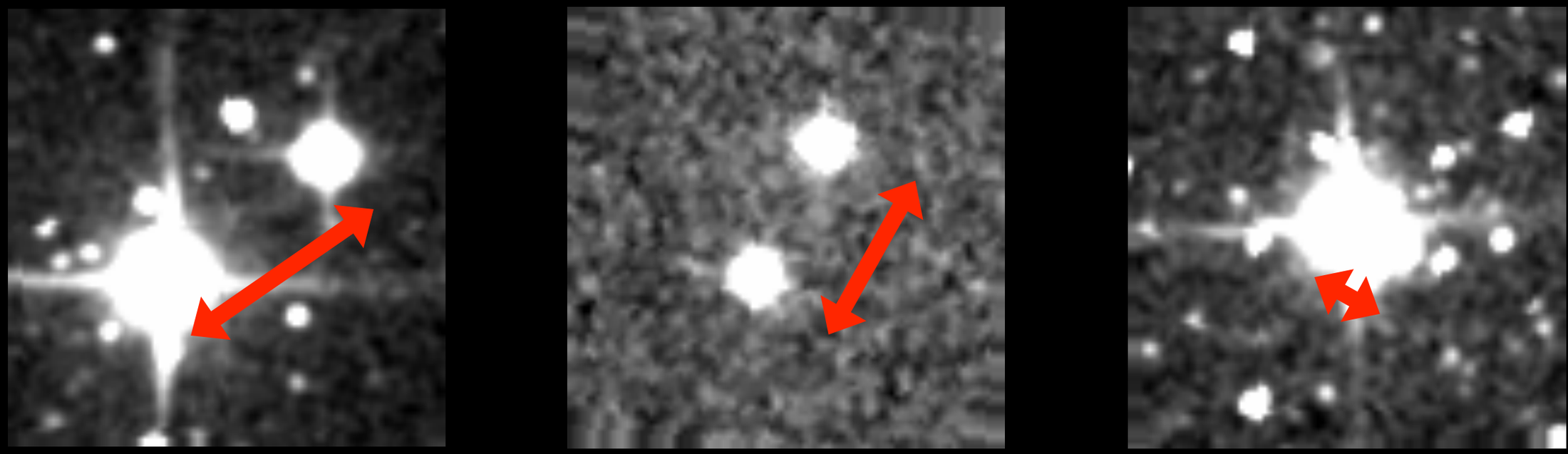

42.6"	31.2"	11.4"

2MASS

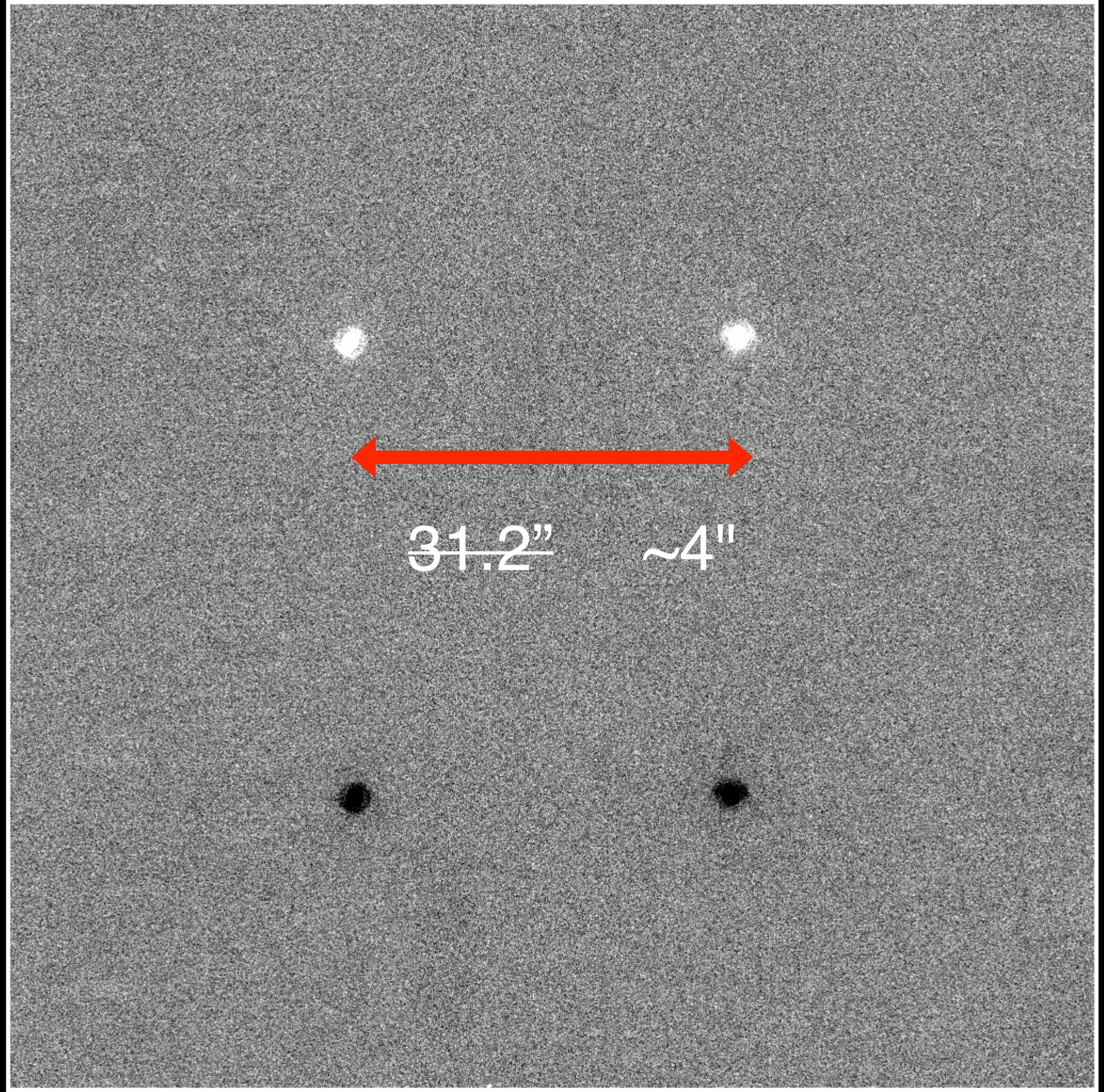
31.2”
~4"

Constant Targets

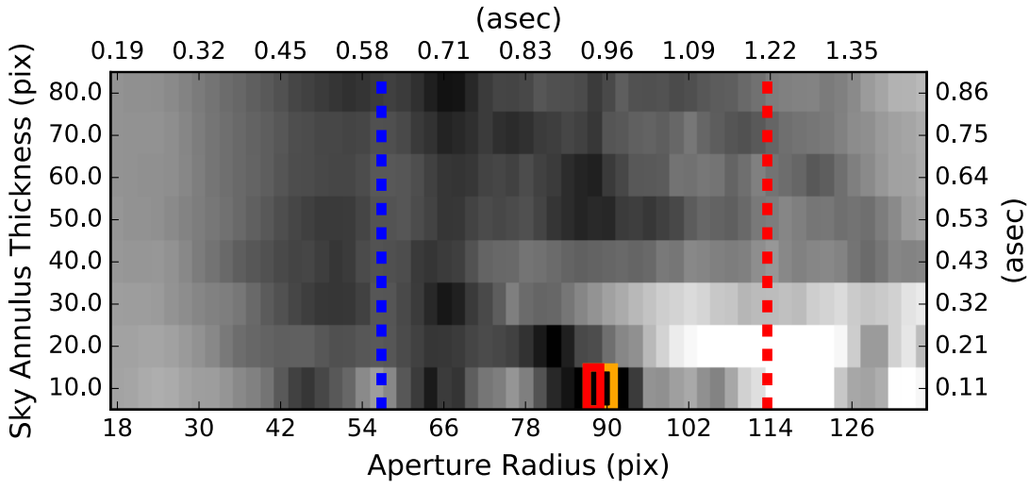

HD 189733 b Secondary Eclipse

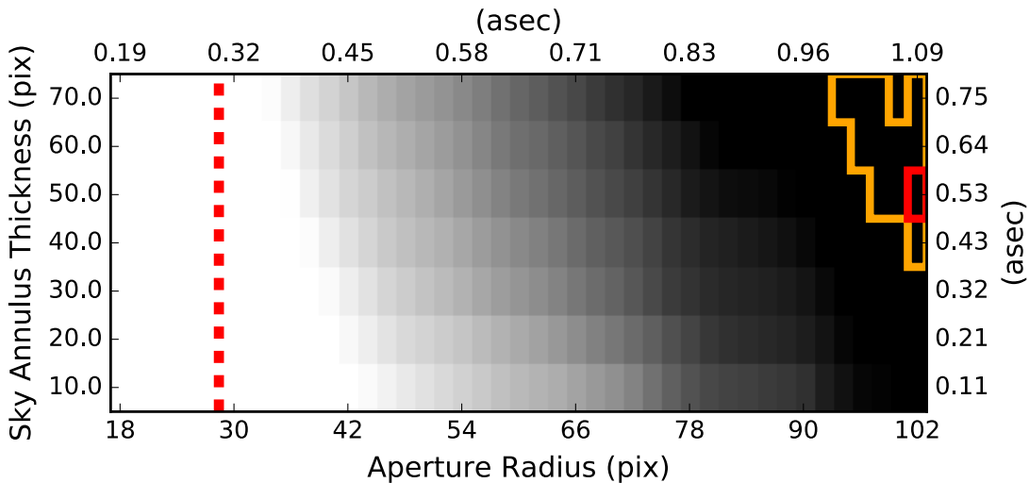

XO-2N b Primary Transit

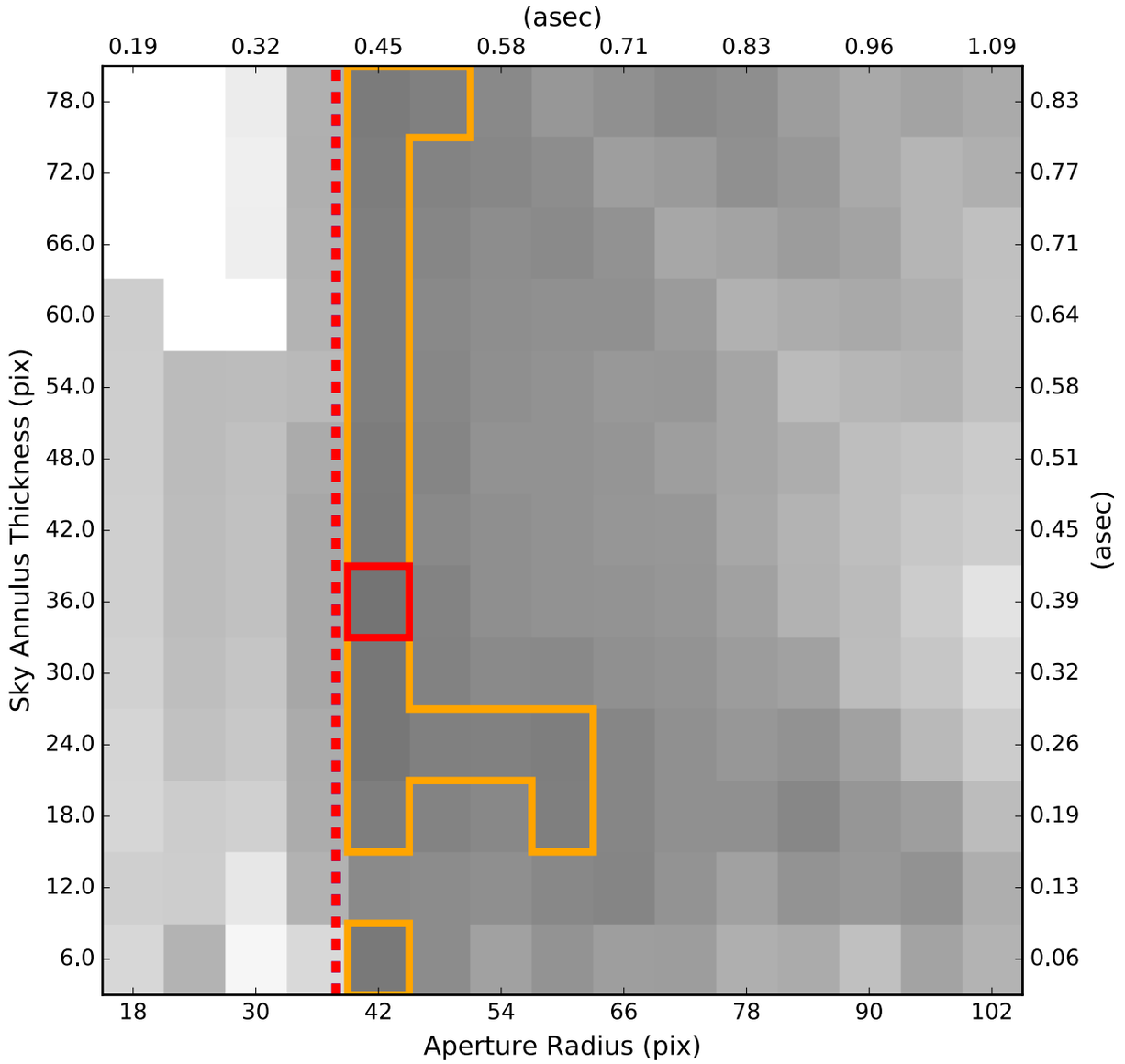

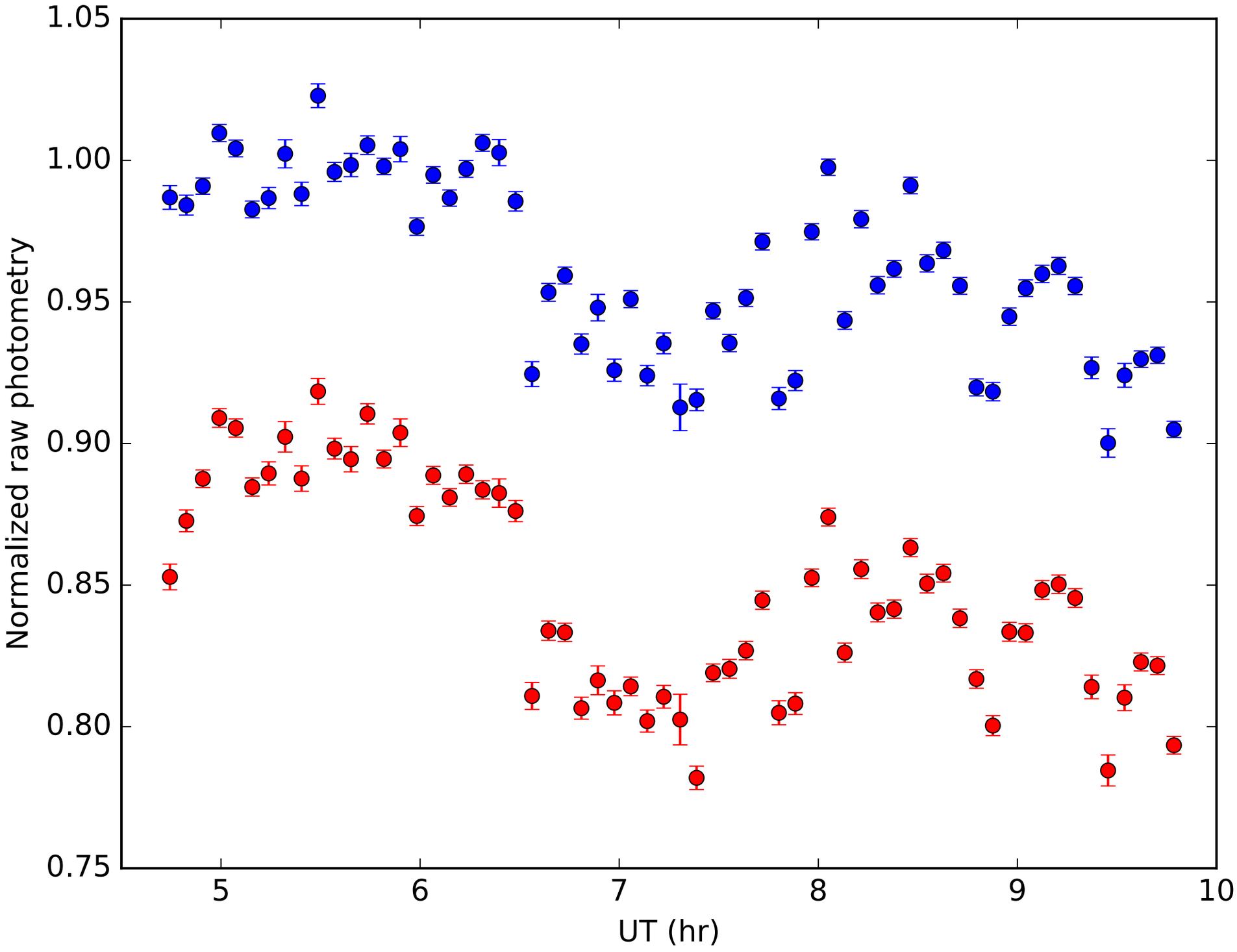
1.05
1.00
0.95
0.90
0.85
0.80
0.75
Normalized raw photometry
5
6
7
8
9
10
UT (hr)

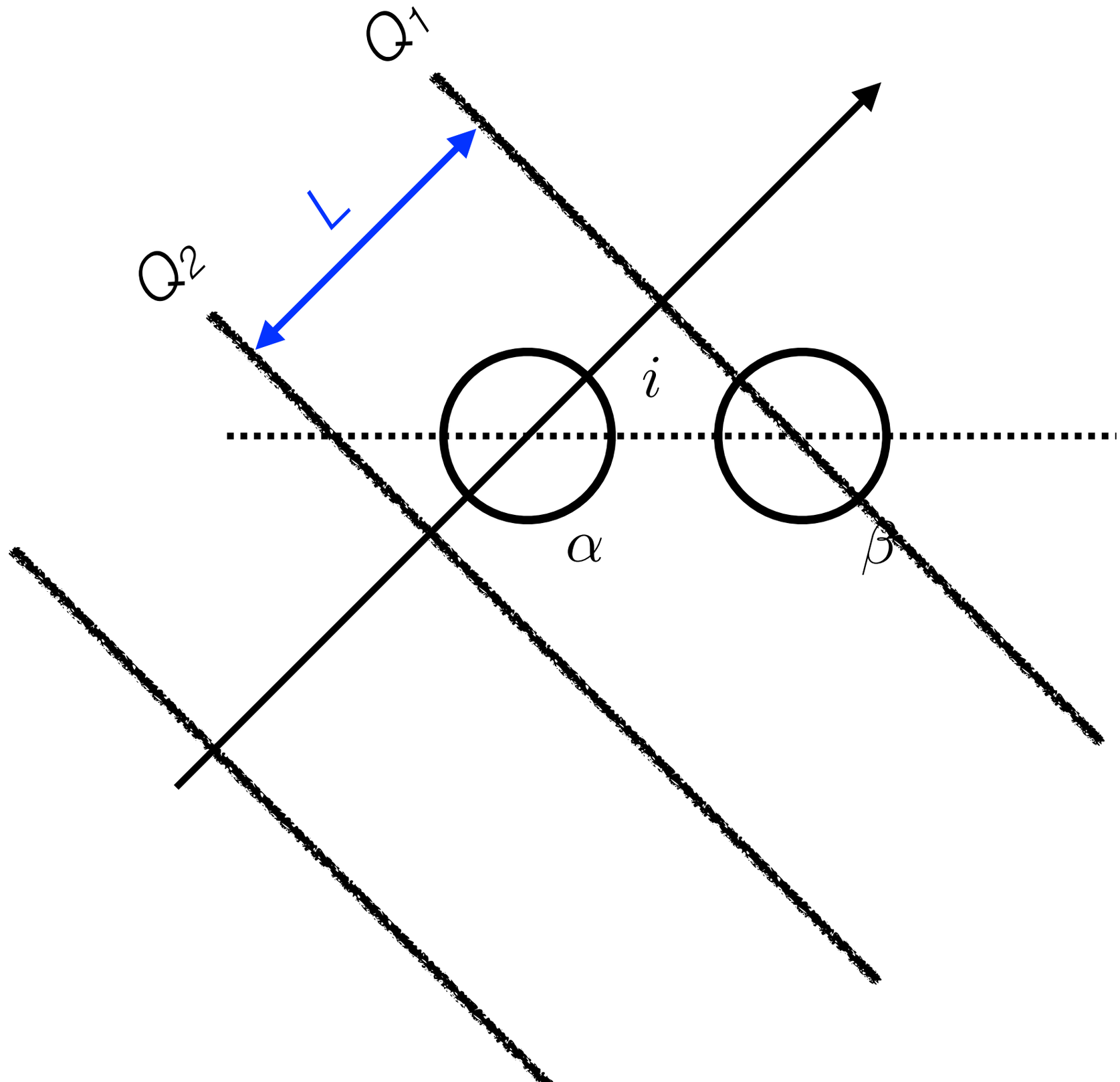
Q1
Q2
L
i
α
β

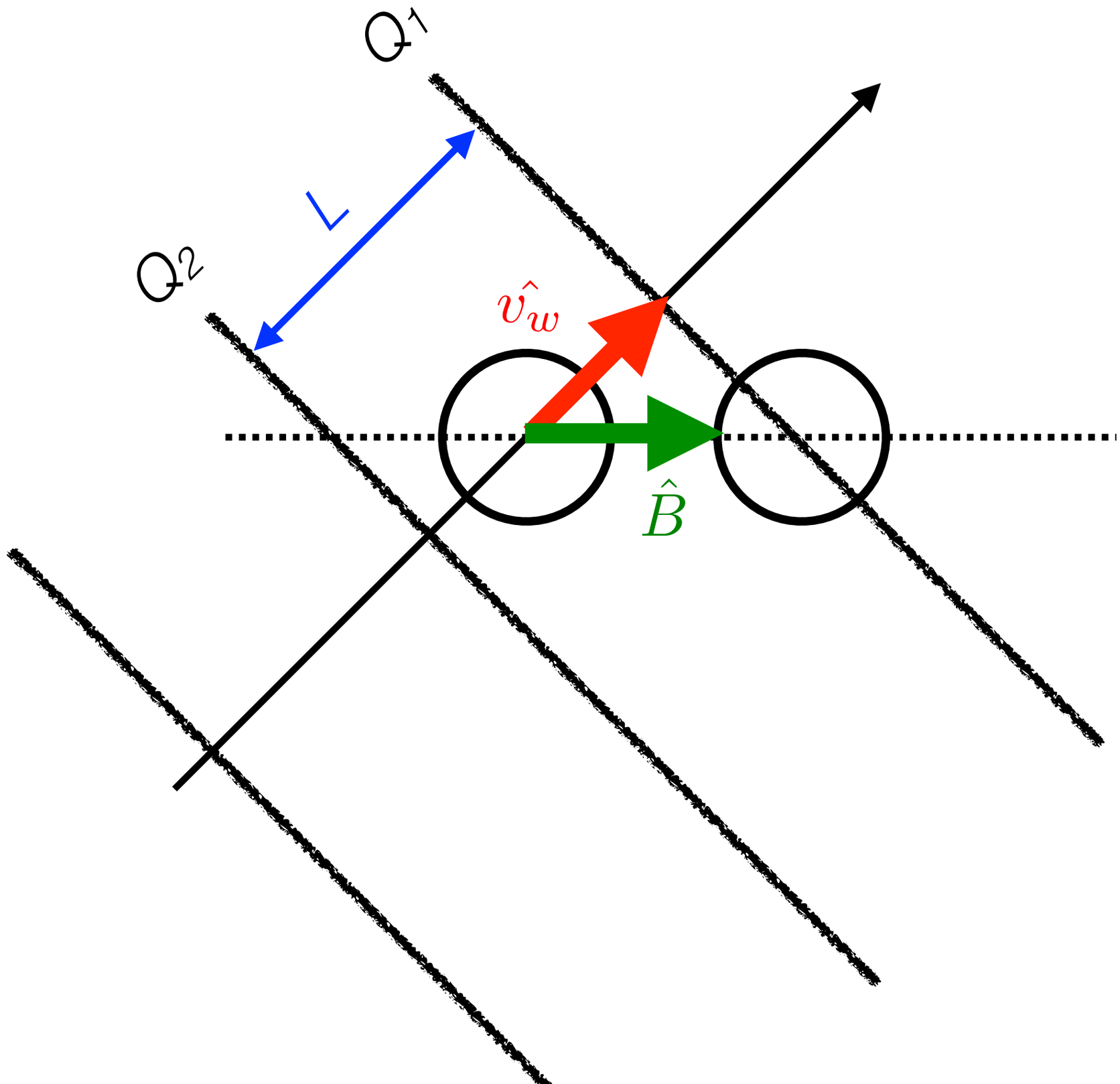
Q1
Q2
L
$\hat{v}_w$
$\hat{B}$

$$F_{tot} = \underbrace{F_{sys}}F_{mod}$$

$$F_{sys}(t) = \left[1 + c_1 + \left(\frac{c_2 t}{hr}\right)\right](1 + c_3 + c_4\Phi\{\overrightarrow{v_w}, \hat{B}; t\})$$

$$F_{tot} = \underbrace{F_{sys}}F_{mod}$$

$$F_{sys}(t) = \left[1 + c_1 + \left(\frac{c_2 t}{hr}\right)\right](1 + c_3 + c_4 \underbrace{\Phi\{\overrightarrow{v_w}, \hat{B}; t\}})$$

$\Phi = 0$ $\Phi \propto \hat{v_w} \cdot \hat{B}$ $\Phi \propto \overrightarrow{v_w} \cdot \hat{B}$

1 2 3

Constant target dataset

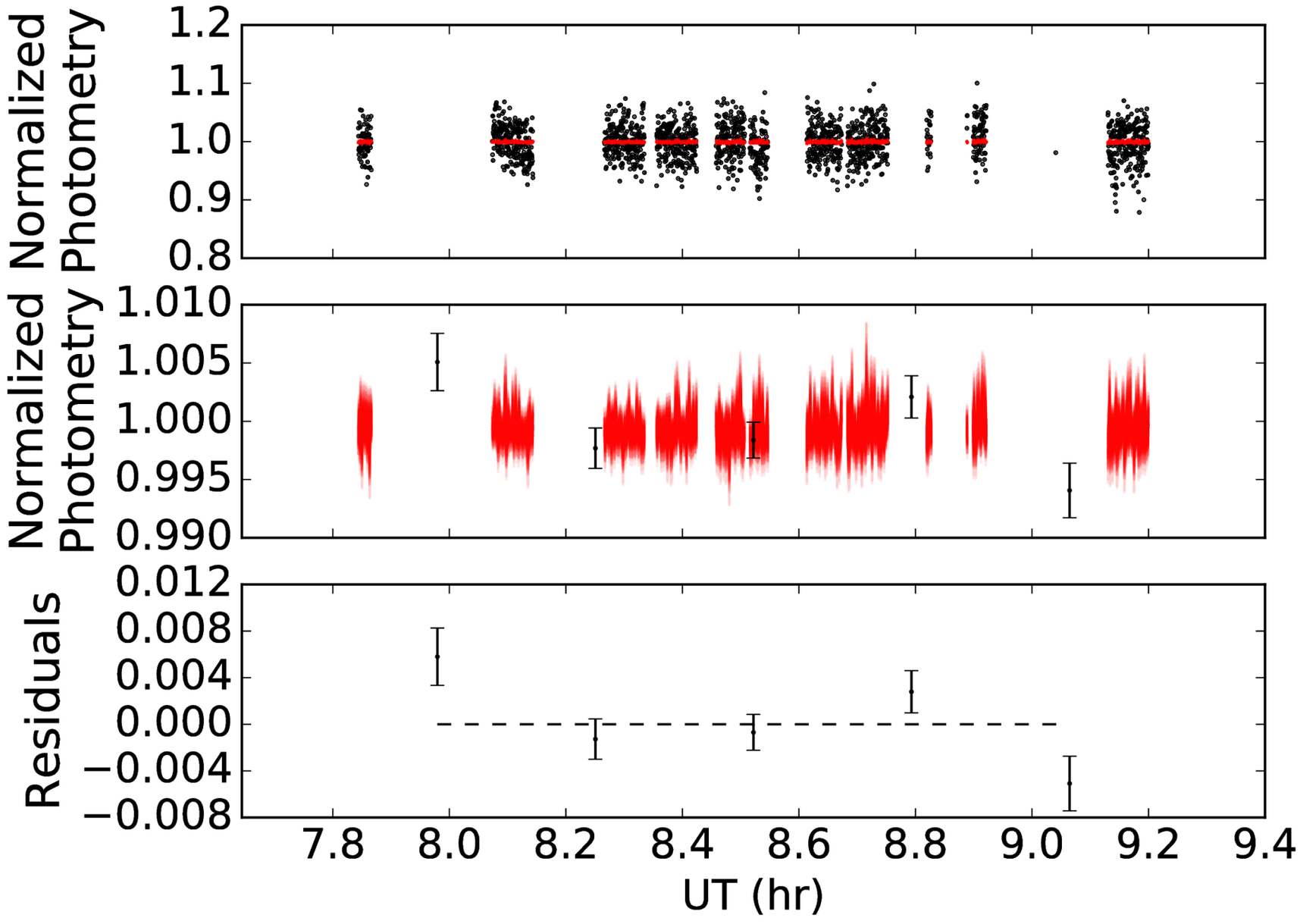

Secondary eclipse dataset

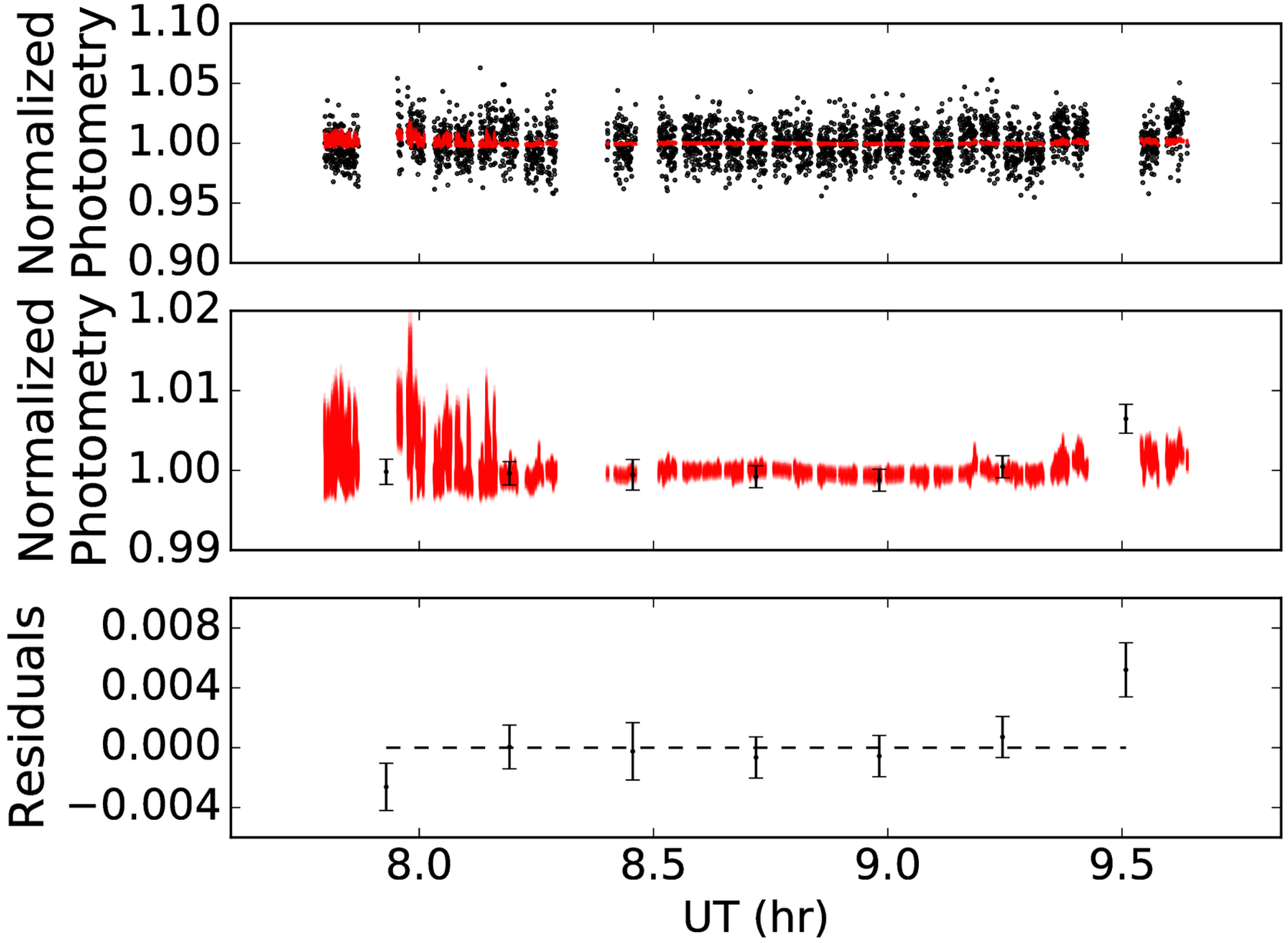

Primary transit dataset

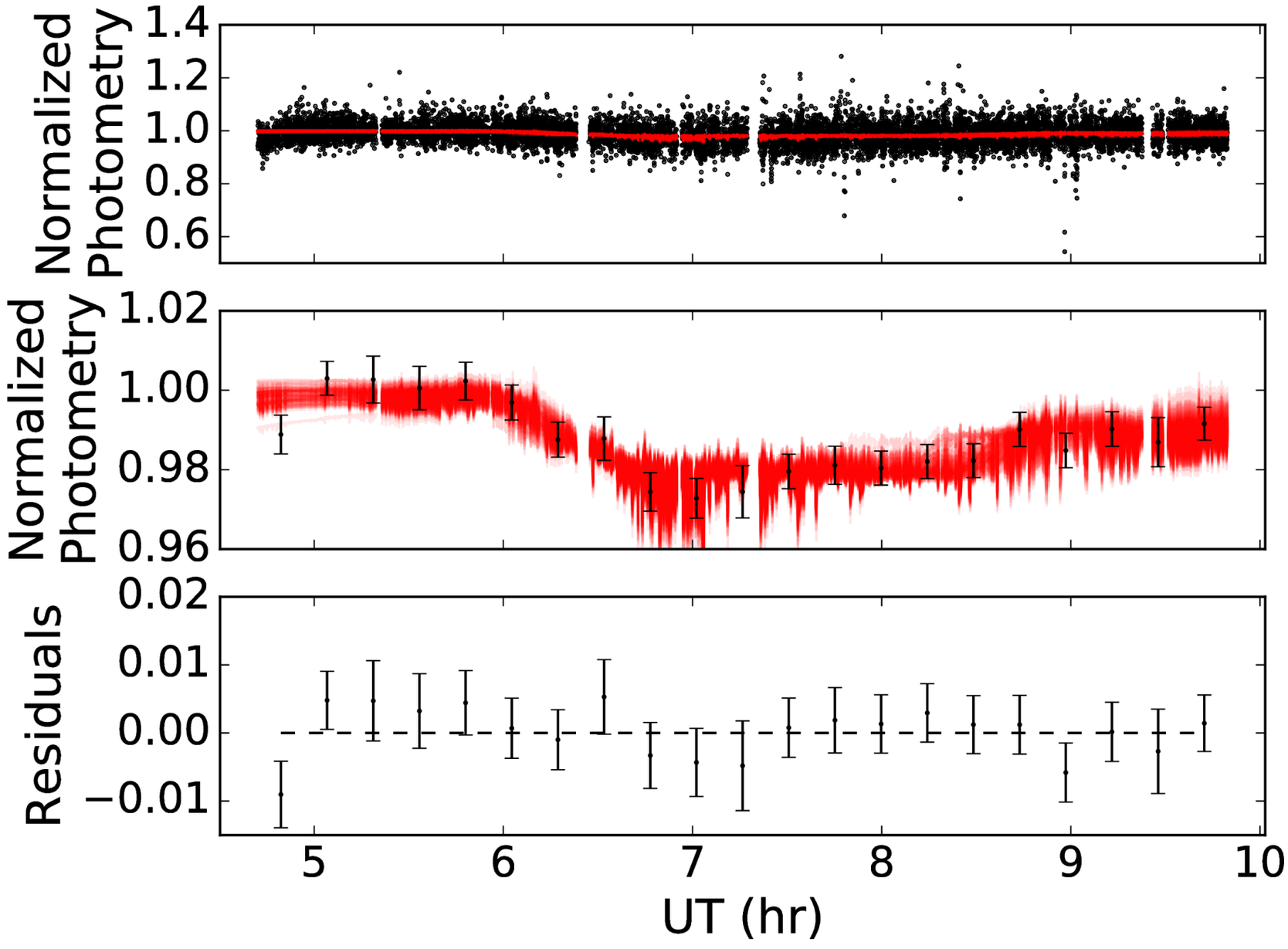

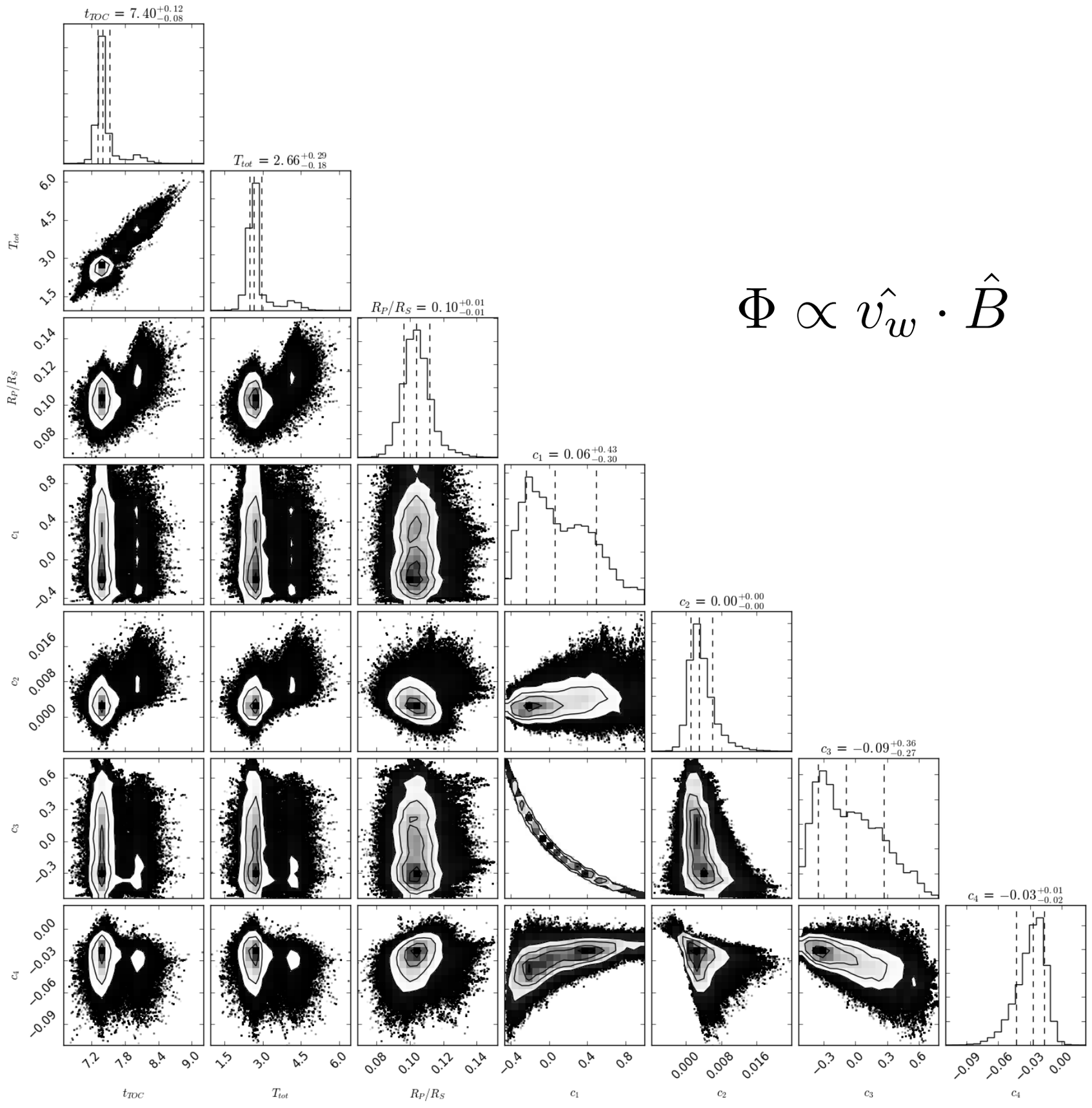

$$\Phi \propto \hat{v_w} \cdot \hat{B}$$

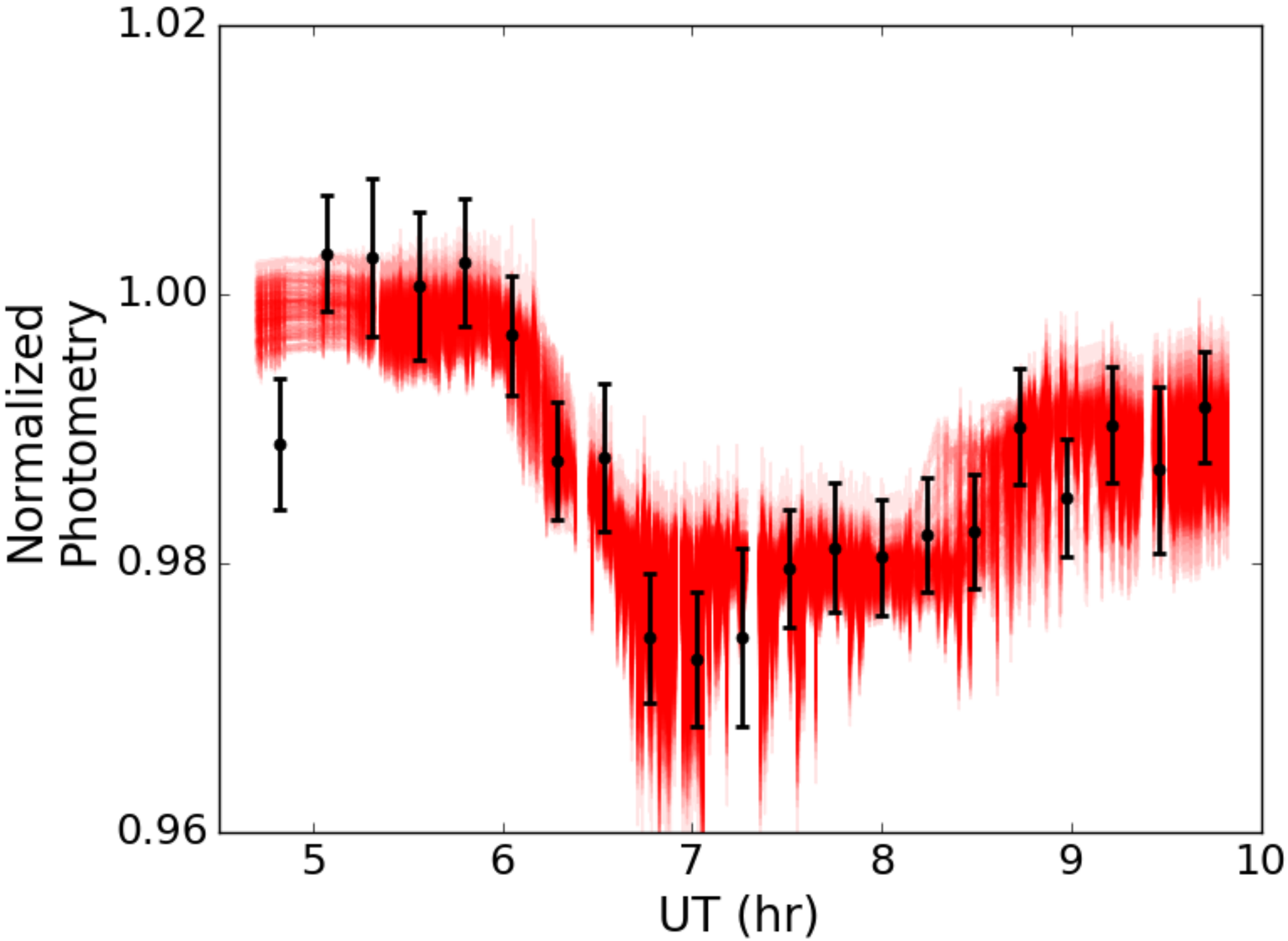
1.02
1.00
0.98
0.96
Normalized
Photometry
5
6
7
8
9
10
UT (hr)

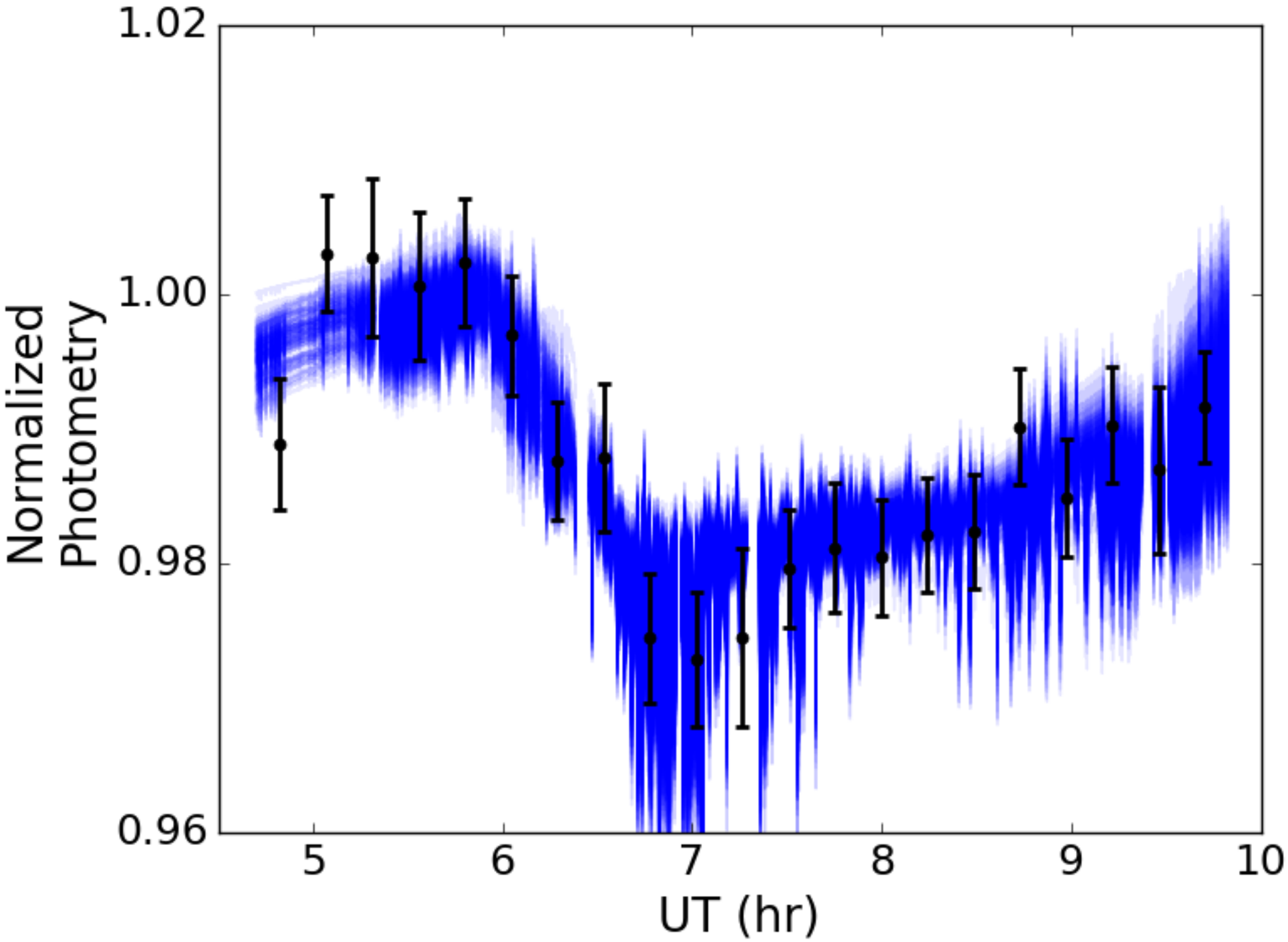
1.02
1.00
0.98
0.96
Normalized
Photometry
5
6
7
8
9
10
UT (hr)

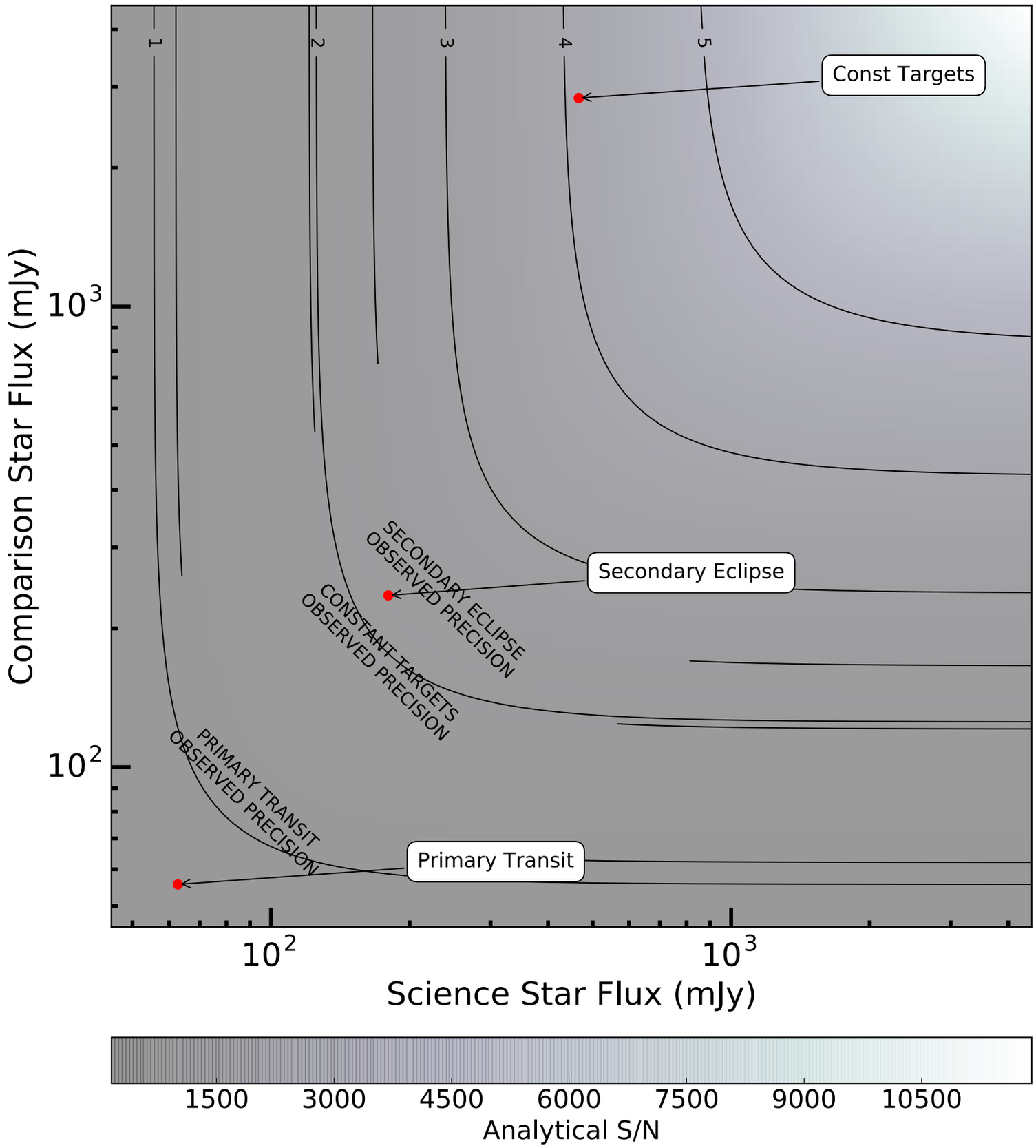
Const Targets
Secondary Eclipse
Primary Transit
SECONDARY ECLIPSE OBSERVED PRECISION
CONSTANT TARGETS OBSERVED PRECISION
PRIMARY TRANSIT OBSERVED PRECISION
1
2
3
4
5
10^3
10^2
10^2
10^3
Comparison Star Flux (mJy)
Science Star Flux (mJy)
1500
3000
4500
6000
7500
9000
10500
Analytical S/N

With comparison star:

$$R_P/R_S = \sqrt{\Delta F} = 0.1036^{+0.0080}_{-0.0072}$$

Without comparison star:

$$R_P/R_S = 0.1980^{+0.0055}_{-0.0049}$$

Dataset	Fit	σ'_{Nmax} (mmag)
Constant targets	LM, $\Phi = 0$	2.2
	MCMC, $\Phi = 0$	2.2
	MCMC, $\Phi = \hat{v_w} \cdot \hat{B}$	2.2
	MCMC, $\Phi = \overrightarrow{v_w} \cdot \hat{B}$	2.2
XO-2N b transit	LM, $\Phi = 0$	4.8
	MCMC, $\Phi = 0$	3.6
	MCMC, $\Phi = \hat{v_w} \cdot \hat{B}$	3.5
	MCMC, $\Phi = \overrightarrow{v_w} \cdot \hat{B}$	3.6
HD 189733 b sec. eclipse	LM, $\Phi = 0$	1.5
	MCMC, $\Phi = 0$	1.5
	MCMC, $\Phi = \hat{v_w} \cdot \hat{B}$	1.3
	MCMC, $\Phi = \overrightarrow{v_w} \cdot \hat{B}$	1.3

Dataset	Fit	σ'_{Nmax} (mmag)
Constant targets	LM, $\Phi = 0$	2.2
	MCMC, $\Phi = 0$	2.2
	MCMC, $\Phi = \hat{v_w} \cdot \hat{B}$	2.2
	MCMC, $\Phi = \overrightarrow{v_w} \cdot \hat{B}$	2.2
XO-2N b transit	LM, $\Phi = 0$	4.8
	MCMC, $\Phi = 0$	3.6
	MCMC, $\Phi = \hat{v_w} \cdot \hat{B}$	3.5
	MCMC, $\Phi = \overrightarrow{v_w} \cdot \hat{B}$	3.6
HD 189733 b sec. eclipse	LM, $\Phi = 0$	1.5
	MCMC, $\Phi = 0$	1.5
	MCMC, $\Phi = \hat{v_w} \cdot \hat{B}$	1.3
	MCMC, $\Phi = \overrightarrow{v_w} \cdot \hat{B}$	1.3

~4 mmag precision in Ls-band

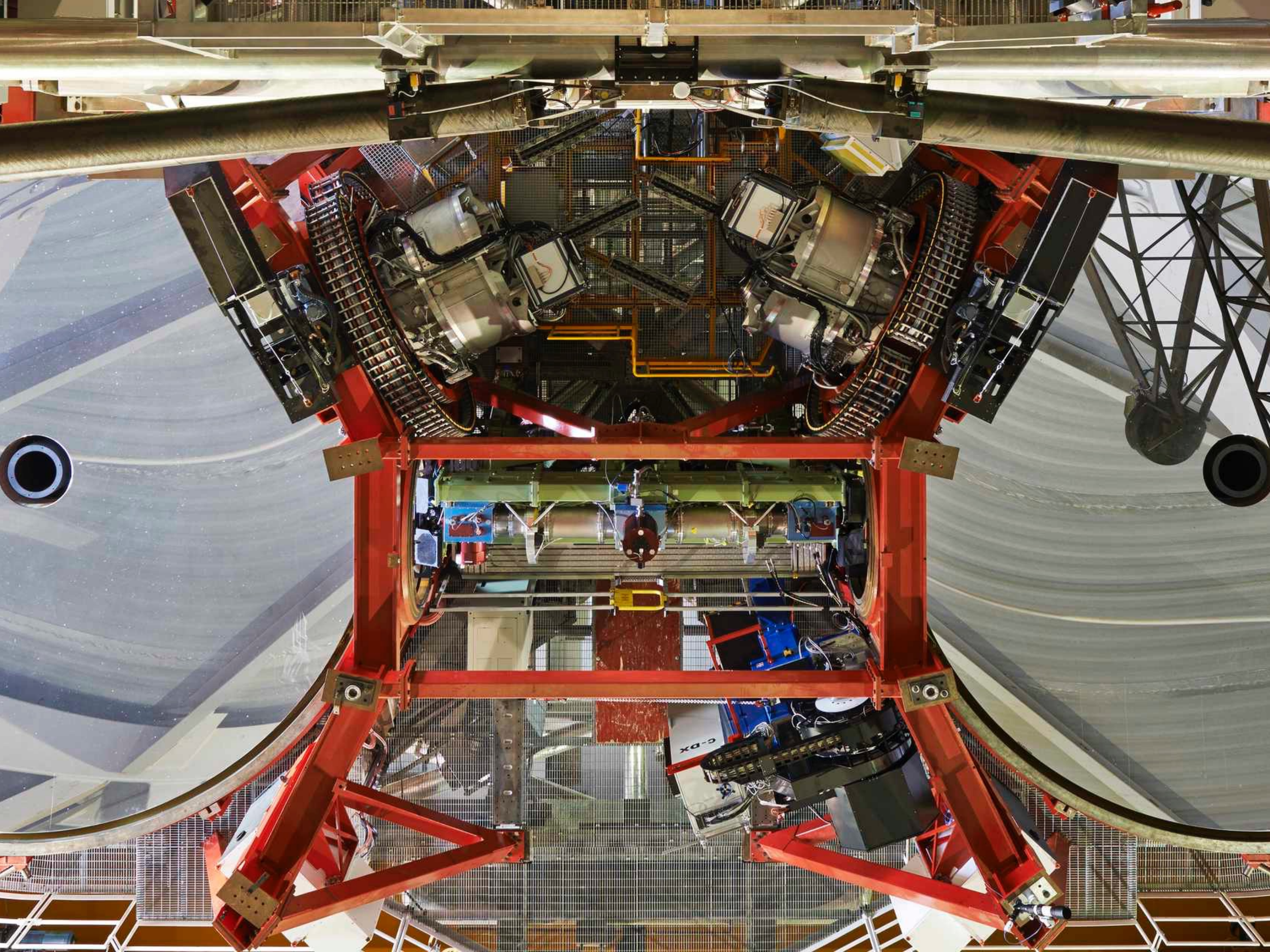

JUNE 16, 2017
using LaTeX style AASTeX6 v. 1.0

PRECISION TIME-SERIES PHOTOMETRY IN THE THERMAL INFRARED WITH A 'WALL-EYED' POINTING MODE AT THE LARGE BINOCULAR TELESCOPE

ECKHART SPALDING[1], PHIL HINZ[1], ANDREW SKEMER[4], JOHN HILL[2], VANESSA P. BAILEY[3], AMALI VAZ[1]

[1]Steward Observatory, University of Arizona, 933 North Cherry Ave. Tucson, AZ 85721, USA
[2]University of Arizona, Large Binocular Telescope Observatory, 933 North Cherry Ave., Tucson, AZ 85721, USA
[3]Kavli Institute for Particle Astrophysics and Cosmology, Stanford University, Stanford, CA 94305, USA
[4]Department of Astronomy and Astrophysics, University of California, Santa Cruz, 95064, USA

ABSTRACT

Time-series photometry taken from ground-based facilities is improved with the use of comparison stars due to the short timescales of variability induced by the atmosphere. However, the sky is bright in the thermal infrared (3-5 μm), and the correspondingly small fields-of-view of available detectors make it highly unusual to have a calibration star in the same field as a science target. Here we present a new method of obtaining differential photometry by simultaneously imaging a science target and a calibrator star, separated by $\lesssim$2 amin, onto a 10×10 asec^2 field-of-view detector. We do this by taking advantage of the LBT's unique binocular design to point the two co-mounted telescopes apart and simultaneously obtain both targets in three sets of observations. Results indicate that the achievable scatter in L_S-band (3.3 μm) is ∼4 mmag for bright targets.

Keywords: methods: observational — techniques: photometric — instrumentation: adaptive optics —instrumentation: miscellaneous — telescopes: individual (LBT)

1. INTRODUCTION

Photometry in the thermal infrared (3-5 μm) has a number of potential applications associated with exoplanetary systems at various stages of their evolution. The thermal infrared probes circumstellar disk material at hundreds of Kelvin in the inner $\lesssim$10 AU of the disk, and water ice has a wide rovibrational transition band at ∼3 μm that can provide constraints on debris disk dust composition (Henning & Semenov 2013; Rodigas et al. 2014). Infrared emission can also be a signature of stellar accretion and mass loss (Polsdofer et al. 2015).

Rapid-cadence, time-series photometry is particularly valuable for placing constraints on the atmospheric composition and vertical structure of brown dwarfs and mature exoplanets. This is done by observing flux variations on the timescales of the rotation periods of brown dwarfs, or the passage of an exoplanet in front of (or behind) its host star (Winn 2010; Buenzli et al. 2012). For example, the L- and L_S-bands can allow the characterization of a methane bandhead in the atmospheres of either brown dwarfs or giant planets, and can help infer the presence of disequilibrium chemistry (Skemer et al. 2012, 2014).

However, attempts to make precise measurements at these wavelengths face a number of obstacles. Space-based facilities are currently limited to the 'warm' Spitzer missions' 3.6 and 4.5 μm broadband channels, which are insufficient to overcome some degeneracies in atmospheric models (Kammer et al. 2015). Ground-based observations, on the other hand, are plagued by systematic effects due to the Earth's atmosphere (e.g., Croll et al. (2015)). Time-series photometry in the thermal infrared is particularly challenging to obtain from the ground due to two interlocking factors: the brightness and variability of the combined backgrounds of the telescope and atmosphere, and the small fields-of-view of detectors sensitive to these wavelengths. The detector fields-of-view (∼few 10 asec across) tend to be restricted so as to spread the photons more thinly across the array and avoid rapid saturation of the pixels, and also to finely sample adaptive-optics-corrected PSFs. AO correction acts to minimize the sky footprint beneath the PSF and thereby minimize the sky component of the noise in strongly background-limited observations. This means, however, that even if the substantial background effects can be decorrelated from the science signal by utilizing a bright comparison star, the tiny fields-of-view conspire to make it unlikely that such stars will be available.

One option is to slew the telescope from the science target to a comparison star and back (e.g., Stephens et al. (2001); Deming et al. (2007)), but this incurs a loss of observing efficiency and fails to capture correlated variability on timescales shorter than the integration or